Published in final edited form as:
J Control Release. 2013 November 28; 172(1): 86–95. doi:10.1016/j.jconrel.2013.06.036.

Inhalation Delivery of Telmisartan Enhances Intratumoral Distribution of Nanoparticles in Lung Cancer Models

Chandraiah Godugu[1], **Apurva R. Patel**[1], **Ravi Doddapaneni**[1], **Srujan Marepally**[1], **Tanise Jackson**[2], and **Mandip Singh**[1,*]

[1]Department of Pharmaceutics, College of Pharmacy and Pharmaceutical Sciences, Florida A & M University, Tallahassee, Florida-32307

[2]Division of Research - Animal Welfare and Research Integrity, Florida A & M University, Tallahassee, Florida-32307

Abstract

The purpose of the present study was to evaluate the effect of Telmisartan (Tel) and Losartan (Los) on nanoparticle intratumoral distribution and anticancer effects in lung cancer. A549 lung tumor cells were orthotopically and metastatically administered to Nu/nu mice. Fluorescent polystyrene nanoparticles (FPNPs, size ~200 nm) beads were used to study their intratumoral distribution after Tel and Los treatments. Animals were administered with FPNPs and after 2h, FPNPs intratumoral distribution was studied by fluorescent microscopy. Tel (~1.12 mg/kg) and Los (~4.5 mg/kg) was administered by inhalation delivery at alternative days for 4 weeks to tumor bearing animals. Collagen-1, transforming growth factor beta 1 (TGF-β1), cleaved caspase-3, Vimentin and E-Cadherin expressions were studied by western blotting. To correlate the AT_1 receptor blockage to anticancer effects, VEGF levels and microvessel densities (MVD) were quantified. Los and Tel treated group resulted in the 5.33 and 14.33 fold increase respectively in the FPNPs intratumoral distribution as compared to the controls. Tel treatment attenuated 2.23 and 1.70 fold Collagen 1 expression compared to untreated control and Los groups, respectively. Further, in Tel and Los treated groups, the TGF-β1 active levels were significantly ($p<0.05$) decreased. Tel (at four times less dose) was 1.89 and 1.92 fold superior in anticancer activity to Los respectively in A549 orthotopic and metastatic tumor models ($p<0.05$) when given by inhalation route. Tel, by virtue of its dual pharmacophoric nature could be an ideal candidate for combination therapy to improve the nanoparticle intratumoral distribution and anticancer effects.

Keywords

Inhalation; Nanotherapeutics; Intratumoral Distribution; Telmisartan; Collagen

1. Introduction

Non-small cell lung carcinoma (NSCLC) is a highly heterogeneous disease and the most common cause of cancer mortality worldwide with a 5-year survival rate of only 15%.

*Corresponding author: Mandip Singh Sachdeva, Professor and Department Head Pharmaceutics, College of Pharmacy and Pharmaceutical Sciences, Florida A&M University, Tallahassee, FL, USA-32307, mandip.sachdeva@gmail.com; Phone # (850)-561-2790; Fax: (850)-599-3813.

Despite recent advances in cancer treatments, the clinical outcome among NSCLC patients is not impressive [1–2]. Chemotherapeutic drugs are rarely successful due to limited amount of the drug reaching the lung tumor cells, resistance development and the associated adverse side-effects [3]. Some of the biopharmaceutical and formulation hurdles in the anticancer drug delivery have been successfully overcome by novel drug delivery systems including nanoparticle approach [4–5]. Cancer chemotherapy that uses nanocarriers has been developed to improve the clinical treatment of solid tumors by obtaining selective high accumulation of drugs in tumor tissues with limited accumulation in normal tissues [6–7]. Cell penetrating peptides, monoclonal antibodies and tumor cell specific nanoparticles can induce targeted delivery of chemotherapeutic agents to tumor cells [4, 8]. However, irrespective of the targeting nature of the nanoparticles, their intratumoral distribution is hindered by dense collagen network and highly fibrous interstitium observed in the solid tumors [9–11]. Solid tumors are characterized by pathologic desmoplasia resulting in increased extracellular matrix (ECM) deposition and tumor fibrosis [11–12]. The ECM is mainly composed of collagen networks and is responsible for the compartmentalization of tumors [12]. Increased ECM remodeling and stiffening by collagen and fibronectin enhances tumor cell survival and proliferation [13–14]. Tumor fibrosis correlates with the progression and invasion of various cancer types [14]. The increased ECM deposition directly contributes to tumor growth by stimulating tumor cell proliferation, increasing angiogenesis, and promoting invasion [15]. In addition to tumor progression, tumor fibrosis also plays crucial role in the intratumoral delivery and distribution of macromolecules. High interstitial fluid pressure, found in various types of tumors is associated with vessel leakiness, lymph vessel abnormalities, and perivascular fibrosis, leading to matrix rigidity and fibroblast contractility and resulting in increased fiber tension. This leads to decreased transcapillary transport and limiting the chemotherapeutic drug delivery to tumors [15].

Use of antifibrotic agents has been reported to decrease tumor interstitial fibrosis and promote nanoparticle intratumoral distribution [6, 10]. The role of transforming growth factor beta (TGF-β1), a multifunctional cytokine in tumor fibrosis has been well documented and plays a pivotal role in regulation of progression of cancer through effects on tumor microenvironment as well as on cancer cells [16–17]. TGF-β system acts as a tumor suppressor in early stages and as a tumor promoter in late stages of tumor progression. Most lung cancers have intact TGF-β signaling but develop resistant mechanisms against TGF-β mediated growth inhibition, suggesting the tumor-promoting role of TGF-β. Expression of TGF-β is frequently upregulated in NSCLC and many other cancers and is correlated with enhanced invasion and metastasis [18]. TGF-β inhibitors have recently been shown to prevent the growth and metastasis of certain cancers [19–20]. Improvement of nanocarriers cancer-targeting therapy by inhibition of TGF-β signaling was also reported in intractable solid tumors [21]. Peroxisome Proliferator-Activated Receptor-γ (PPAR γ) activation also inhibited the tumor metastasis by antagonizing TGF-β and Smad3 [18, 22]. A recent study demonstrated that AT_1 receptor blocker Los through TGF-β inhibition improved the penetration and therapeutic efficacy of drug loaded nanoparticles [10]. Tel, another AT_1 blocker also demonstrated PPAR γ activity and several studies demonstrated the beneficial effects of Tel over other AT_1 blockers [23–25]. Previous studies have also suggested the role of Tel in controlling diabetes associated cardiovascular complications by virtue of its additional PPAR γ agonistic activity [26]. Further, Tel has also been reported to reduce TGF-β induced ECM production in various disease conditions [23, 27]. The combined antifibrotic effects of PPAR γ activators and AT_1 receptor blockers (ARB) may be more beneficial in ameliorating tumor fibrosis which could be successfully used with Tel [28–30].

Angiotensin II (Ang-II) is the biologically active peptide of the renin-angiotensin system (RAS) involved in blood pressure control, tissue remodeling and angiogenesis as well as in vascular and inflammatory pathologies. However, compelling evidence indicates that the

Ang-II peptides also play a role in cell proliferation and metastasis [31]. Ang-II is a vasoconstrictor, a mitogen, and an angiogenic factor, while angiotensin (1–7) has vasodilator, anti-proliferative, and anti-angiogenic properties [32–35]. Major functions attributed to Ang-II (inflammation, angiogenesis and migration) are also related to cancer progression [31]. Most components of the RAS including angiotensinogen, angiotensin converting enzyme (ACE) and angiotensin receptors are expressed locally in a wide variety of tumors [31, 36]. Angiogenesis is essential for tumor growth and metastasis and vascular endothelial growth factor (VEGF) is the most potent angiogenic factor identified to date and is produced by RAS through AT_1 receptor activation [37]. TGF-β1 acts as an indirect angiogenic agent by regulating the VEGF production [38]. Recently various reports have demonstrated the anticancer effects of angiotensin receptor (AT_1) blockers (ARBs) and AT_2 receptor activators and Ang 1–7 peptides [13, 34, 39–41]. Considering the important role of AT_1 receptors in tumor development and metastasis, and signal cross talk between TGF-β1, AT_1 receptors in tumor fibrosis [42], the current study has been designed to study the antifibrotic effects of Los and Tel in Lung cancer models [42]. Tumor fibrosis nature was characterized by estimating collagen levels and masson trichrome staining. Role of TGF-β1 in collagen induced tumor fibrosis was studied by quantifying the TGF-β1 levels. The mechanism of anticancer effects induced by Los and Tel were characterized by analyzing the apoptosis (cleaved caspase 3) and MMP-9 expressions. The role of ARBs on tumor angiogenesis was studied by VEGF and microvessel density (MVD) levels. Further, the antimetastatic effects of Los and Tel were studied by Vimentin, E-Cadherin and MMP-9 expressions.

In this study, we have proposed to treat the lung tumors with Los and Tel by inhalation route prior to administering the nanoparticles to solid lung tumors. We hypothesize that prior treatment with Tel will make poorly penetrable fibrous tumors into easily nanoparticle penetrable loose interstitial networks allowing for better intratumoral distribution of the nanotherapeutics leading to their superior anticancer effects.

2. Materials and methods

2.1. Materials

Tel, Los were purchased from Alpha Aesar (MA 01835), and Fluorescent polystyrene sulphate modified Latex beads (L9902-1 ML) were procured from Sigma Aldrich (St. Louis, MO 63178). Human non-small cell lung cancer cells (A549 and H1650) and normal lung fibroblasts WI-38 were procured from ATCC. The antibodies (TGF-β1 was from R&D systems MN 55413), Collagen-1, Cleaved caspase-3, CD31, E-cadherin, AT_1 receptor (F-3) Vimentin and MMP-9 were procured from Santa Cruz Biotechnology Inc (CA 95060). VEGF kit was purchased from Thermo Fisher scientific Inc (IL 61101). TGF-β1 ELISA kit was purchased from R&D systems (MN 55413). Masson trichrome staining kit was purchased from Polysciences Inc (PA 18976).

2.2. In vitro anticancer effects of Los and Tel

Non-small cell lung cancer cell lines A549 and H1650 were plated in 96 well plates at 10,000 cells/well density. After 24h, cells were treated with various concentrations of Tel and Los, 0.1 % DMSO treated cells were considered as control cells. After 72h the treatment, cells were fixed in 0.25% gultaraldehyde and stained with 0.05% crystal violet staining. Percent of cell viability or cell kill was calculated by considering DMSO treated control cells as 100% viable (zero % cell kill).

2.3. Effect of Los and Tel on normal lung fibroblasts

To study the effect of Tel on normal lung fibroblast cells (WI-38), dose dependent cytotoxic effects were studied. 10,000 cells/well were plated in 96 well plates and allowed to attach and grow for 24h, then cells were treated with different doses of Los and Tel (in DMSO). After 72h of treatment, cytotoxicity was studied by crystal violet staining method. Percent of cell viability or cell kill was calculated by considering DMSO treated control cells as 100% viable (zero % cell kill).

2.4. Aerodynamic size distribution analysis

Particle size distribution was measured using an 8-stage Anderson cascade impactor, Mark II connected to the PARI LC STAR jet nebulizer mouth piece. The impactor plates were coated with 10% Pluronic L10 in ethanol solution to prevent particle bounce. The aqueous formulation or solution was nebulized using PARI LC STAR jet nebulizer using dry compressed air for 5 min into the cascade impactor which was operated at a flow rate of 28.3 L/min according to USP guidance [43]. To determine the aerodynamic properties of Los and Tel, the inhaled aerosol on the nebulizer, throat, jet stage, plates on impactor stages 0–7, and filter was collected by washing with 5 ml of HPLC grade water. The analysis of Los and Tel was performed on a Waters HPLC system using a Symmetry C18 column (5 μm, 4.6 × 250mm) with a Nova-Pack C8 guard column at corresponding wavelengths and flow rate of 1 ml/min. The HPLC system consisted of a Waters autosampler (model 717 plus), Waters binary pump (model 1525), and Waters UV photodiode array detector (model 996). All samples were analyzed in triplicate. The mass median aerodynamic diameter (MMAD) and geometric standard deviation (GSD) was obtained from impactor data using established software. Impactor experiments were repeated at least two times. Data was expressed as the percentage of the total drug deposited on all stages of the impactor including actuator and throat and represent mean ± sem (n=3).

2.5. Inhalation delivery of Tel and Los

Water soluble Los was dissolved in Phosphate buffer saline. Aqueous formulations of Tel suitable for nebulization were prepared by dissolving the drug in Hydroxyl propyl beta-cyclodextrin solution. These solutions were used for in vitro characterization and for animal inhalation studies. The total amount of Los and Tel deposited into each mouse was calculated based on the earlier reported method [43]. The estimated total deposited amount of inhaled Los and Tel (D) for the ambient air was calculated by the following formula:

$$D = C \times V \times DI \times T \quad (1)$$

Where; C = concentration of Los (500 μg/ml) or (Tel 125 μg/ml) in aerosol volume, V = volume of air inspired by the animal during 1 min [for mice, V = 1.0 L-min/kg], DI = estimated deposition index [fraction of inhaled dose deposited throughout the respiratory tract (for mice DI = 0.3)], T = Duration of treatment in min (T = 30 min).

One week after the tumor cell injections, animals were grouped into control, Tel, Los, FPNPs, Tel+FPNPs and Los+FPNPs. All the Tel and Los group animals were exposed to aerosolized form of Tel (125 μg/ml) and Los (500 μg/ml) with a PARI LC STAR jet nebulizer using dry compressed air at a flow rate of 4.5 L/min for 30 min by nose only inhalation exposure system. Mice were restrained in animal holders and placed in an inhalation chamber (SCIREQ, Montreal, Canada), such that only the nose of each mouse was exposed to the aerosol cloud. The nebulizer was connected to the top part of the inhalation chamber from which the generated aerosol flowed down the central tower to the 12 mice peripherally arranged. Inhalation was performed every alternative day for 2 weeks. After the last inhalation dose, fluorescent nanoparticles were given i.v. via tail vein. Animals

were sacrificed by high dose of CO_2 and tumors along with lungs were isolated and used for the microscopic studies to analyze nanoparticle intratumoral distribution. Alternatively, some tissues were either stored in −80°C for western blotting or fixed in formalin saline for Immunohistochemistry, histopathology and masson trichrome staining. In separate set of animals, inhalation delivery was continued for 4 weeks to study the anticancer effects of Tel and Los in orthotopic and metastatic tumor models.

2.6. Animals

The laboratory murine model has been used extensively in lung cancer research. Female, 6-week old, athymic Nu/nu mice were purchased from Harlan Inc. (Indianapolis, IN). The mice were housed and maintained in specific pathogen-free conditions in a facility approved by the American Association for Accreditation of Laboratory Animal Care. Food and water were provided ad libitum to the animals in standard cages. Animals were maintained at standard conditions of 37°C and 60% humidity. All experiments were done in accordance with the guidelines of the Institutional Animal Care and Use Committee (IACUC) at Florida A&M University. Animals were acclimatized for 1 week prior to the tumor studies.

2.7. Orthotopic and Metastatic tumor models

A549 cells were grown in F12K Media containing 10% FBS and standard antibiotic mix at 5% CO_2 and 37°C. For orthotopic lung tumor model, mice were anesthetized with Isoflurane and a 5 mm skin incision was made to the left chest, 5 mm below the scapula. Hamilton syringes (1 ml) with 28-gauge hypodermic needles were used to inject the cell inoculums through the sixth intercostal space into the left lung. The needle was quickly advanced to a depth of 3 mm and quickly removed after the injection of the A549 cells (2 million per mouse) suspended in 100 μL PBS (pH 7.4) into the lung parenchyma. Only cell suspensions of >95% viability as determined by tryphan blue exclusion were used. Wounds from the incisions were closed with surgical skin clips. Animals were observed for 45 to 60 min until fully recovered. These animals develop lung cancer within 14 days after the cell inoculation. Female athymic nude mice (six week-old) were used for metastatic lung cancer model by administering A549 cells (2 million per mice) intravenously by tail vein administration. Untreated mice were used as control and other groups were treated either by inhalation delivery of Tel, Los or FPNPs or both nanoparticles according to the study design.

2.8. Intratumoral distribution of Nanoparticles

After last dose of inhalation administration of Tel or Los, animals were intravenously administered with 100 μL of FPNPs. After 2h, animals were sacrificed and lungs along with tumors were collected. Part of the tumors was fixed in formalin solution for histopathology and immunohistochemical studies. Frozen tissues were embedded in OCT medium and cryosectioned. 10 μm sections were mounted on the microscopic slides, the red fluorescence generated from FPNPs was visualized and qualitative nanoparticle intratumoral distribution was analyzed by ImageJ software. Average of 10 fields was studied for each slide. For each tissue, three slides were prepared and for each group 3 tissues were analyzed.

2.9. Western blot analysis

Protein was extracted from tumor tissues collected from control-untreated and treated tumors using RIPA lysis buffer (50mM Tris-HCL, pH 8.0, with 150 mM sodium chloride, 1.0% Igepal CA-630 (NP-40), 0.5% sodium deoxychlorate, and 0.1% sodium dodecyl sulfate) with protease inhibitor and 500 mM phenylmethylsulfonyl fluoride. Protein content was measured using BCA Protein Assay Reagent Kit (PIERCE, Rockford, IL). Equal amounts of supernatant protein (50 μg) from the control and different treatments were

denatured by boiling for 5 min in SDS sample buffer, separated by 10% SDS-PAGE, transferred to nitrocellulose membranes for immunoblotting. Membranes were blocked with 5% skim milk in Tris-buffered saline with Tween 20 [10mM Tris-HCL (pH 7.6), 150 mM Nacl, and 0.5% Tween 20] and probed with antibodies against Collagen 1 (COL-1) (1:500), TGF-β1 (1:500), E-Cadherin(1:500), Vimentin(1:500), AT_1 receptor (1:500) and β-actin (1:1000). Horseradish peroxidase-conjugated secondary antibodies (Santa Cruz Biotechnology, Santa Cruz, CA) were used. Proteins were visualized using enhanced chemiluminescent solution (Pierce, Rockford, IL) and exposed to Kodak X-OMAT AR autoradiography film (Eastman Kodak, Rochester, NY).

2.10. Histopathology and Masson trichrome staining

Both orthotopic and metastatic lung tumors were processed for normal histopathological procedures and 5–10 μm sections were made. After deparaffinization and rehydration, sections were stained with Hematoxylin and Eosin for normal histological evaluation. Masson trichrome staining was performed to localize the collagen distribution in the tumors. Collagen staining was performed according to the manufacturer's kit procedures (Polysciences, lnc). The blue color staining indicates the presence of collagen fibers in the tumor.

2.11. Assessment of anticancer efficacy

The general physiological behavior and body weight profiles of mice were recorded during the study. Animal survival rates were recorded. At the end of studies (five weeks post tumor implantation or injection), all mice were sacrificed and the lung weight, tumor weight, tumor volume, number and volume of tumor foci (central, mid and peripheral region) were determined; excised lung and tissue samples were stored at –80°C for further analysis by western blotting and immunohistochemistry (IHC).

2.12. IHC for Cleaved caspase 3, Microvessel density (MVD) and MMP-9

Formalin fixed tumors were processed for automatic histopathological procedures. Tissue sections were dehydrated by immersing in increasing concentrations of alcohol and embedded in paraffin. Paraffin embedded specimens were cut into thin sections (5–10 μm). Tissue sections (4–5 μm thick) mounted on poly-L-lysine–coated slides and sections were deparaffinized with xylene and rehydration through graded concentrations of alcohol, then incubated with 3% hydrogen peroxidase for 20 min to block endogenous peroxidase activity. Antigen retrieval for Cleaved caspase-3, CD31 and MMP-9 staining was carried out for 10 min in 0.01 M sodium citrate buffer (pH 6), heated at 95°C in a steam bath followed by cooling for 30 min. Endogenous peroxidase was blocked by 3% hydrogen peroxide in PBS for 10 min. The slides were washed with PBS and incubated for 1 h at room temperature with a protein blocking solution. Excess blocking solution was drained, and the samples were incubated overnight at 4°C with cleaved caspase-3, CD31 and MMP-9 antibodies or incubated with biotinylated secondary antibody followed by streptavidin. The color was developed by exposing the peroxidase to a substrate-chromagen, which forms a brown reaction product. The sections were then counterstained with hematoxylin. Cleaved caspase-3, CD31 and MMP-9 expression was identified by the brown cytoplasmic staining. Numbers of positive cells per filed was quantified by counting 10 different fields from each section.

2.13. Quantification of VEGF and TGF-β1 by ELISA

VEGF and TGF-β1 levels were estimated in plasma, tumor tissue homogenates and in vitro cell culture supernatant samples from sub-confluent A549 cell cultures by ELISA. Tumors were homogenized in RIPA lysis buffer (20 mM Tris-HCl pH 7.5, 150 mM NaCl, 1% Triton

X-100) containing proteinase inhibitors (Complete Proteinase Inhibitor Cocktail Tablets, Roche, Indianapolis. IN). Tissue debris was pelleted and the resulting supernatant was used in subsequent analysis. Total protein concentration was determined with a BCA protein assay (Pierce, Rockford, IL). For in vitro estimations, media was collected 48h after the treatments. VEGF concentrations were determined according to the manufacturer's instructions. Total and active TGF-β1 levels were measured by TGF-β1 Quantikine® ELISA kit according to the manufacturers protocol (R&D Systems, Minneapolis, MN). A monoclonal antibody specific for TGF-β1 was pre-coated onto microplates. To activate latent TGF-β1 to immunoreactive active TGF-β1 recommended protocol was followed. The TGF-β1 levels estimated in native samples indicated the active form. The difference in the TGF-β1 levels between activated and native samples indicate the total TGF-β1 levels. A minimum of 4 tumors per group were analyzed in duplicate.

2.14. Tumor size and volume analysis

The lung weights and tumor volume were used for assessment of therapeutic activity of the treatments. We also evaluated efficacy of therapy in different areas by determining average number of tumor nodules in central, mid and peripheral region of lungs harvested from metastatic control and treated groups. Tumor nodules of 2–10 mm^3 in volume were counted using photo microscope (ProgRes C10 plus, Olympus, USA).

2.15. Statistics

All data are presented as the mean ± standard error of the mean (sem). Statistical differences were evaluated by Student's t-test or one way analysis of variance (ANOVA) followed by Tukey's test. The criterion for statistical significance was set at $p<0.05$.

3. Results

3.1. In vitro anticancer effects of Tel and Los

The IC_{50} values for Tel and Los with A549 cells were 80.37±10.64 μM and 210.46±15.67 μM, respectively. Similar pattern of activity was observed in H1650 cells, IC_{50} values for Tel and Los being 60.71±5.82 μM and 224.65±16.83 μM, respectively (Figure 1A). The cell proliferation assays revealed that both Tel and Los inhibited the cell proliferation dose dependently; further Tel exhibited increased inhibition on cell proliferation compared to Los (Figure 1B). Both Tel and Los up to 200 μM concentration did not exhibit significant cytotoxic effects with human normal lung fibroblasts, WI-38 (Figure 1C).

3.2. Aerodynamic size distribution analysis for inhalation characterization and lung deposition

Assessment of size and shape characteristics of Tel and Los aerosolized formulations were assessed by determining their mass median aerodynamic diameter (MMAD), fine particle fraction (FPF) and geometric standard deviation (GSD) using Anderson Mark-II cascade impactor. Tel formulation yielded FPF of 71.6 ± 4.6%, MMAD of 1.8 ± 0.23 μm and GSD of 1.5 ± 0.27. Similarly, Los formulation yielded FPF of 69.7 ± 5.9%, MMAD of 1.6 ± 0.31 μm and GSD of 1.8 ± 0.19. With Spraytec, the Tel formulation showed Dv_{50} of 2.51 μm with FPF of 73.84 ± 3.64% indicating that the aerodynamic values are well in agreement with that of cascade impactor values and more than 70 % of aerosolized droplets were below 5 μm. Based on initial experiments, the concentrations of solutions used for inhalation exposure were 0.5 mg/ml for Los and 0.125 mg/ml for Tel. The in vitro theoretical lung deposition experiments suggested that total amount of Los and Tel deposited into each mouse was 4.5 mg/kg and 1.12 mg/kg, respectively. Therefore, the doses used for the inhalation studies were fixed as 4.5 mg/Kg for Los and 1.12 mg/Kg for Tel.

3.3. Effect of Tel and Los Inhalation delivery on Intratumoral distribution of Nanoparticles

In control tumors, the nanoparticle intratumoral penetration was limited and confined to areas around blood vessels (Figure 2A). Administration of Los and Tel by inhalation for 2 weeks, significant increase in the distribution of FPNPs was evidenced by observed intense and uniform distribution of nanoparticles in treated groups (Figure 2A). The quantitative fluorescent data indicated significant improvement in the intratumoral distribution in Tel group compared to Los and untreated control groups. When compared to control tumors, Los and Tel treated group resulted in the 5.33±0.21 and 14.33±1.87 fold increase respectively in the nanoparticle intratumoral distribution. Interestingly, Tel showed 2.7±0.34 fold increase in the nanoparticles intratumoral distribution compared to Los (Figure 2D). When studied the FPNPs distribution in 6 weeks inhalation exposed animals, similar type of significant increase in the nanoparticle intratumoral distribution was observed (supplementary data SIII B).

3.4. Effect of tumor fibrosis on nanoparticle intratumoral distribution and effect of Tel and Los on tumor fibrosis

The fibrous nature of lung tumor was studied by estimating the tumor Collagen 1 levels. Since, TGF-β1 is responsible for the synthesis of Collagen 1, the role of TGF-β1 levels in tumor fibrous nature and effect of Tel and Los were studied. Collagen 1 levels were quantified by western blot and densitometric analysis suggested that compared to untreated control, Los treatment significantly reduced the tumor Collagen 1 expression by 1.31 fold in orthotopic tumors. Further, Tel treatment significantly attenuated Collagen 1 expression (2.23 and 1.70 fold) compared to untreated control and Los groups, respectively (Figure 3A). Further, in metastatic tumors, Tel produced superior collagen1 inhibition than the Los (Figure 3B). Western blot analysis of active TGF-β1 expressions suggested that activated forms of TGF-β1 levels were over expressed in orthotopic lung tumors and Tel and Los treatment resulted in its significant reduction (Figure 3C). Further, the active and latent forms of TGF-β1 levels analyzed by ELISA method revealed that the increased levels of active form (Phosphorylated) were detected in untreated A459 cell culture supernatants. Total TGF-β1 levels were found to be not significantly different except in Tel 30 μM treated A549 cells. Further Los and Tel (10 and 30 μM) resulted in significant reduction in the activeTGF-β1 levels suggesting that both Los and Tel inhibit the TGF-β1 activation (Figure 3D). Significant increase in the active TGF-β1 levels were found in lung tumor lysates and plasma collected from untreated control animals compared to Tel and Los groups. The total amount of TGF-β1 was found to be unaltered in the control and Los groups, whereas in Tel treated group significant reduction in the total TGF-β1 levels were found (Figure 3E&F). These results indicating that Los by inhibiting the TGF-β1 activation and Tel by decreasing the TGF-β1 expression as well as activation may leads to collagen synthesis inhibition. TGF-β1 active levels were significantly decreased in Los ($p<0.05$) and Tel ($p<0.001$) treated groups, indicating the crucial role of TGF-β1 activation in tumor fibrosis and the antifibrotic effects of Tel and Los observed to be through inactivation of TGF-β1, in turn leading to reduction in the tumor collagen levels.

3.5. Histopathology and Masson trichrome staining

Histological evaluation of tumor sections by H&E staining showed the presence of dense fibrillar networks distributed intratumorally. These extracellular networks divided the tumor into several compartments (red arrows). Whereas in Tel and Los treated tumors, these extracellular networks disappeared (Figure 4). The extracellular matrixes are made up of collagen was measured by collagen specific masson trichrome staining. Significant amount of collagen was deposited in both orthotopic and metastatic lung tumors (Figure 5A). The compartmentalization seen in H&E stained control tumor sections was also further

demonstrated by collagen staining in orthotopic tumors, which clearly indicated the role of collagen in the tumor fibrosis. Inhalation treatment with Tel and Los significantly reduced collagen distribution in the tumors. The quantitative analysis of collagen expression in orthotopic and metastatic tumor models revealed that Los produced 2.71 and 2.60 fold reduction, respectively. Compared to untreated controls, Tel treatment showed 4.35 and 5.44 fold reduction in the collagen expression in orthotopic and metastatic tumor models, respectively. Further, Tel produced 1.60 and 2.08 fold reduction in the collagen levels in orthotopic and metastatic tumor models, respectively compared to Los treated groups (Figure 5B); this observation confirms the superior effects of Tel over Los in controlling the tumor collagen expression.

3.6. Effect of Tel and Los inhalation delivery in orthotopic and metastatic lung tumors

The inhalation delivery of Tel and Los on alternative day exposure for 4 weeks showed significant reduction in the lung weights in orthotopic and metastatic tumor models. In orthotopic models, lung weights together with tumor were 519.51±55.13 mg in untreated control groups, whereas in Los and Tel treated animals the lung weights were found to be 359.58±36.82 and 246.48±15.25 mg, respectively (Figure 6A). Similarly, in metastatic tumor models also lung weights were significantly reduced with Los and Tel treatment (Figure 6A). The lung tumor volumes in control, Los and Tel treated groups were 578.50±55.5 mm3, 391.5±39.0 and 231.25±37.64 mm3, respectively (Figure 6B). Tel treated lung weights were significantly lower (1.89 and 1.92 fold, in orthotopic and metastatic models, respectively) than the Los groups, clearly indicating that Tel has superior anticancer effects than Los.

Further, number of tumor nodules was counted in central, mid and peripheral lobes from metastatic tumor models to analyze the metastatic nature of the lung tumors. In all three lobes, the number of tumor nodes was found to be significantly decreased in Los and Tel treated groups compared to untreated control animals, suggesting that both Los and Tel exhibit antimetastatic anticancer effects (Figure 6C). Further, Tel produced superior anticancer effects than Los in both orthotopic and metastatic tumor models (Figure 6A–C). The survival rates of orthotopic and metastatic tumor bearing animals were increased in Los and Tel treated groups. In orthotopic lung tumor animals the survival rates were found to be 33.33% for untreated control groups, further, Los and Tel treatment resulted in the increase in the survival to 66.66 and 83.33%, respectively. Similarly, the survival rates in metastatic tumor bearing animals were also increased from 33.33% (in control) to 83.33% in Los treated animals, whereas in Tel treated animals 100% survival rate was recorded (Figure 6D). There was no significant change in the body weights were observed in both the tumor models treated with Los and Tel, suggesting the safety of the inhalation delivery of Los and Tel (Figure 6E&F). Our extended inhalation exposure of Los and Tel for 6 weeks also resulted in significant reduction in the lung tumor weights; however, even the maximum possible duration of inhalation exposure in our models (6 weeks) did not eradicate the lung tumors completely, suggesting that Los or Tel treatment only decrease the tumor weights up to some extent, however, the complete eradication of tumors with these treatments is not possible (Supplementary data SIII).

3.7. Effect of Tel and Los treatment on apoptosis, VEGF levels and microvessel density (MVD)

Since Ang-II receptor blockers, ARB Los and Tel showed anticancer effects in lung cancer models, the role of apoptosis, angiogenesis and VEGF in ARB induced anticancer activity was studied. IHC analysis of lung tumor sections suggested that Los and Tel treatment resulted in significant increase in the cleaved caspase 3 positive apoptotic cells (Figure 7A), indicating the role of apoptosis. IHC analysis of lung tumor sections showed that MVD was

significantly increased in untreated control lung tumors. Treatment with Tel and Los resulted in the significant reduction (1.75 and 3.85 fold) in the MVD (Figure 7B) in the orthotopic model while, in case of In metastatic tumor models, Los and Tel produced 1.47 and 1.82 fold reduction in the MVD compared to control groups. Tel produced superior reduction in the vessel density compared to Los and control groups (Figure 7B and 8C). Significant reduction in the MVD was noticed in Los and Tel treated tumors. These observations imply that Tel and Los through angiotensin II receptor blockage exhibit antitumor effects. MMP-9 levels were also significantly reduced in Los and Tel treated groups compared to control orthotopic tumors, indicating the possible role of MMP-9 in tumor fibrosis and progression (Figure 8A).

VEGF levels secreted into the cell culture supernatant was significantly reduced ($p<0.01$) in Los and Tel groups compared to control cells. Both Los and Tel dose dependently reduced the VEGF levels. Tel produced significant reduction in VEGF levels at 10 and 30 μM, compared to corresponding concentrations of Los (Figure 9A). The increased levels of VEGF observed in untreated control (151.10±25.02 pg/ml) tumors were significantly alleviated in Los (98.01±7.35 pg/ml) and Tel (64.03±7.44 pg/ml) groups, indicating that ARBs through VEGF inhibition exert anticancer effect (Figure 9B). Similarly, in plasma also VEGF levels were significantly decreased upon treatment with Los (216.50±18.48 pg/ml) and Tel (100.13±16.92 pg/ml) when compared with control plasma (338.25±42.58 pg/ml) (Figure 9B).

3.8. Effect of Tel and Los treatment on Epithelial and mesenchymal Transition (EMT)

The role of Tel and Los on tumor EMT was studied by western blotting. Los and Tel treatment resulted in the significant reduction in the Vimentin expression. Los reduced 4.56 fold and Tel treatment resulted in 5.77 fold reduction in the Vimentin expression. Another EMT marker E-Cadherin significantly increased in Tel treated group compared to untreated control groups (Figure 9 C&D). The AT_1 receptor expression was significantly down regulated in Tel treated groups compared to control and Los (Figure 9E). This could be possible through PPAR γ activation of Tel.

The toxicity profile in healthy lung tissue surrounding the lung tumors after the long term (4–6 weeks) inhalation exposure of Los and Tel was found to be normal, The fibrolytic effects of Los and Tel did not alter the collagen expression in the normal lung tissues (Supplementary data SI&SII).

4. Discussion

This is the first study to report the antifibrotic effects of Tel and Los in lung cancer models to improve the nanoparticles distribution. In addition, inhalation delivery of Tel and Los per se exhibited potential anticancer effects. The uniqueness of the current study is the inhalation based selective delivery of the fibrolytic agents to lung tumors without unwanted systemic exposure. Schematic representation of our inhalation approach to reduce lung tumor fibrosis is shown in figure 10.

Though the role of fibrosis in nanoparticle distribution has been reported in various tumors types, it was thought that fibrosis originates mostly from the cancer associated fibroblasts (CAF) [44–45]. Howe ver, our in vitro studies with NSCLCs suggest that in addition to CAFs, tumor cells are also involved in the TGF-β1 induced tumor fibrosis [44]. Previous reports suggest that increased extracellular matrix accumulation plays crucial role in tumor metastasis. Furthermore, recent studies also suggest that macromolecular distribution of nanoparticles into the tumor was greatly influenced by the fibrous nature of the tumors [11,

46–47]. This could be one of the main reasons why nanoparticles based anticancer drug formulations have not demonstrated significant benefits upon clinical use.

For inhalation delivery, based on the solubility of the compounds, Los was dissolved in PBS, while Tel was dissolved in water by using hydroxyl propyl β cyclodextrin. MMAD of 0.5–5um and GSD of less than 1.22 are considered optimal for aerosolized drug particles. Thus, relatively respirable polydisperse particles were obtained after nebulization of Tel and Los and adequate deposition was achieved in the lung of mice to exert their antifibrotic and anticancer effects.

Intratumoral distribution studies indicated that in untreated tumors, FPNPs penetration was not uniform and the distribution was confined to only around leaky vasculature. Whereas, in Los and Tel treated tumors, increased penetration and uniform intratumoral distribution of FPNPs was observed. TGF-β1 plays a pivotal role in regulation of progression of cancer through effects on tumor microenvironment as well as on cancer cells and there is a strong correlation between tumor collagen levels and TGF-β1 activation [6, 21]. The increased TGF-β1 activity in in-vitro experiments with A549 cells suggested that tumor cells are also involved in the TGF-β1 induced increased collagen synthesis and tumor fibrosis [6]. Our findings were further supported by a recent study which demonstrated the anticancer and antifibrotic effects of TGF-β1 inhibitors in breast cancer models. Inhibition of TGF-β by soluble receptors or neutralizing antibodies resulted in significant increase in nanoparticle intratumoral distribution and improved nanotherapeutic efficacy [6]. In another study, upon TGF-β blockade, improved nanoparticle extravasation and penetration was reported in pancreatic and other cancers [21, 48]. Our results demonstrated that, despite the dose of Tel (1.12 mg/kg) was 4 times less than Los (4.5 mg/kg), Tel significantly decreased the Collagen 1 levels in orthotopic and metastatic lung tumor models (Figure 4). Activated TGF-β1 level was significantly decreased in Tel treated animals compared to untreated control and Los groups (Figure 4). A recent study demonstrated that Los dose-dependently reduced the stromal collagen in desmoplastic models of human breast, pancreatic, and skin tumor models and improved the penetration and therapeutic efficacy of drug loaded nanoparticles [10]. The Los doses used in the reported studies were 10–60 mg/kg, while corroborating those findings; we observed that Los at the dose of 4.5 mg/kg by inhalation route produced improved nanoparticle distribution. Further Tel when given by inhalation route at a minimal dose of 1.12 mg/kg produced significant fibrolysis and enhanced intratumoral distribution of nanoparticles in lung tumors. Due to selective delivery to lung tumors, the doses required for both Los and Tel are 5–10 fold lesser than the reported studies [10]. Our demonstrated antifibrotic effects with Tel suggest that this approach can be applied to a variety of other tumor types for enhancing nanoparticle delivery and distribution.

Further, during our inhalation studies, we found that after 2 weeks of inhalation delivery (alternative days) of Tel, there was significant reduction in the lung tumor weights compared to vehicle treated control groups, suggesting that there are additional anticancer effects while trying to reduce the tumor fibrosis. Further, estimation of VEGF levels suggested that both Tel and Los reduced VEGF levels. Several reports have suggested the role of Tel as a PPAR γ agonist [28] and it is our hypothesis that this additional mechanism resulted in significant reduction of VEGF levels compared to Los groups. Further, the role of PPAR γ in VEGF and anticancer effects was confirmed from the PPAR γ antagonist GW9662; in presence of this antagonist the anticancer effects and VEGF levels were comparable to Los group (data not shown). These findings suggest that both Los and Tel through AT_1 inhibition reduced VEGF levels which are involved in tumor angiogenesis. Therefore, Tel induced inhibition of tumor cell proliferation observed in our study is mediated through PPAR γ activation [49]. Our in vivo studies further demonstrated significant reduction in the VEGF levels in tumor

homogenates from Tel treated animals compared to vehicle treated control and Los treated animals. Further supporting the data from immunohistochemical analysis showed that cleaved caspases-3 expression was found to be significantly increased in Los and Tel treated animals, suggesting the promising anticancer effects of these agents upon inhalation delivery. The decreased MVD and VEGF levels confirm the anti-angiogenic effects of Los and Tel. The decreased MMP-9 levels further support the antifibrotic effects of these drugs because MMP-9 is one of the important components in the extracellular matrix and is also involved in tumor fibrosis. Therefore, use of FDA approved drugs like Los and Tel currently on the market with strong safety profiles could be beneficial to improve the cancer therapy [32]. Moreover Tel has superior activity over Los possibly through PPAR γ activation. This is supported by the hypothesis that since TGF-β is involved in tumor fibrosis, use of ARBs with additional PPAR γ agonistic activity may show beneficial effects in abrogating the tumor fibrosis which in turn may increase the intratumoral distribution of nanotherapeutics [22]. Although, Los showed significant improvement in nanoparticle distribution and reduction in the lung tumor weights, due to lack of its PPAR γ activation ability, these effects were inferior to Tel. However, if both the active metabolites of Losartan EXP3179 (PPAR γ activator) and EXP 3174 (AT_1 blocker) are combined the similar comparable to Tel results might be possible.

High fibrous nature is also one of the reasons for tumor progression and metastasis. Because, tumor collagen modulates E-Cadherin mediated cell-to-cell contact to increase tumor invasiveness and metastases [15], there is a strong relationship between tumor fibrosis and aggressive nature of that particular tumor [12]. Further, TGFβ1 plays a role in the Epithelial-mesenchymal transition (EMT) process, which is crucial in tumor cell migration and metastasis. Our studies suggested that both drugs inhibit the EMT process by down regulating Vimentin and up regulating the E-Cadherin levels. Further, the role of EMT in tumor fibrosis is also well documented. Therefore, inhibition of TGFβ1, EMT, collagen synthesis pathway by Los and Tel suggest the promising use of these agents in tumor metastasis and fibrosis. The superior effects of Tel to inhibit EMT process can be attributed to its PPAR γ mediated EMT inhibition [18, 50]. Recent clinical data analysis indicated the possible carcinogenic effect of Tel upon chronic use when used for cardiovascular problems. The report suggested that there was a significant increase in the cancer risk in Tel treated patients [51]. This is a very controversial report with several other reports refuting this claim and in contrast to those reports we used Tel (in very low doses) by inhalation for shorter periods (2–4 weeks) to disrupt the tumor extracellular matrix. Our studies clearly demonstrate that Tel exhibits anticancer effects through several mechanisms and has no role in inducing cancers as reported. Since both Los and Tel are safe drugs and dose used for the inhalation studies were very low, no visible signs of toxicity were observed. The H&E and Masson trichrome staining in the healthy tissues suggested that, upon inhalation of Los or Tel did not alter the normal tissues (Supplementary data SI and SII).

Though the current study is addressing the problems associated with nanoparticle intratumoral distribution in high collagen containing fibrous tumors, similar kind of increased tumor fibrosis is possible in several other non-fibrous tumors. Further, even if the tumor is not fibrotic in nature, it was reported that radiation therapy increases tumor fibrosis [52]. Further it is also speculated that AT_1 receptors are also involved in radiation induced fibrosis and in such conditions use of AT_1 receptor blockers may efficiently reduce tumor fibrosis. Our results support the concept that angiotensin receptor blockers with additional PPAR γ activation may be beneficial for controlling TGFβ1-induced tumor fibrosis and metastasis, because PPAR γ also regulates the tumor TGFβ1 expression as well as its activation [22].

5. Conclusions

Tel and Los showed significant anticancer effects in orthotopic and metastatic lung tumor models. Inhalation delivery of Tel produced better antifibrotic effect than Los. Tel, by virtue of its dual pharmacophoric nature could be an ideal candidate for combination therapy to improve the nanoparticle intratumoral distribution and anticancer effects. Tel induced antifibrotic strategy could be used for variety of tumors to improve the efficacy of nanotherapeutics.

Supplementary Material

Refer to Web version on PubMed Central for supplementary material.

Acknowledgments

The authors acknowledge the financial assistance provided by 1) NIH grant number SC1CA161676-01A1 and 2) Financial support from Department of Defense grant number W81XWH-11-1-0211.

References

1. Siegel R, Naishadham D, Jemal A. Cancer statistics, 2012. CA Cancer J Clin. 2012; 62:10–29. [PubMed: 22237781]
2. Molina JR, Yang P, Cassivi SD, Schild SE, Adjei AA. Non-small cell lung cancer: epidemiology, risk factors, treatment, and survivorship. Mayo Clin Proc. 2008; 83:584–594. [PubMed: 18452692]
3. Califano R, Abidin AZ, Peck R, Faivre-Finn C, Lorigan P. Management of small cell lung cancer: recent developments for optimal care. Drugs. 2012; 72:471–490. [PubMed: 22356287]
4. Kim K, Kim JH, Park H, Kim YS, Park K, Nam H, Lee S, Park JH, Park RW, Kim IS, Choi K, Kim SY, Kwon IC. Tumor-homing multifunctional nanoparticles for cancer theragnosis: Simultaneous diagnosis, drug delivery, and therapeutic monitoring. J Control Release. 2010; 146:219–227. [PubMed: 20403397]
5. Sandhiya S, Dkhar SA, Surendiran A. Emerging trends of nanomedicine--an overview. Fundam Clin Pharmacol. 2009; 23:263–269. [PubMed: 19527298]
6. Liu J, Liao S, Diop-Frimpong B, Chen W, Goel S, Naxerova K, Ancukiewicz M, Boucher Y, Jain RK, Xu L. TGF-beta blockade improves the distribution and efficacy of therapeutics in breast carcinoma by normalizing the tumor stroma. Proc Natl Acad Sci U S A. 2012; 109:16618–16623. [PubMed: 22996328]
7. Cho K, Wang X, Nie S, Chen ZG, Shin DM. Therapeutic nanoparticles for drug delivery in cancer. Clin Cancer Res. 2008; 14:1310–1316. [PubMed: 18316549]
8. Gobin AM, Moon JJ, West JL. EphrinA I-targeted nanoshells for photothermal ablation of prostate cancer cells. Int J Nanomedicine. 2008; 3:351–358. [PubMed: 18990944]
9. Cabral H, Matsumoto Y, Mizuno K, Chen Q, Murakami M, Kimura M, Terada Y, Kano MR, Miyazono K, Uesaka M, Nishiyama N, Kataoka K. Accumulation of sub-100 nm polymeric micelles in poorly permeable tumours depends on size. Nat Nanotechnol. 2011; 6:815–823. [PubMed: 22020122]
10. Diop-Frimpong B, Chauhan VP, Krane S, Boucher Y, Jain RK. Losartan inhibits collagen I synthesis and improves the distribution and efficacy of nanotherapeutics in tumors. Proc Natl Acad Sci U S A. 2011; 108:2909–2914. [PubMed: 21282607]
11. Jain RK, Stylianopoulos T. Delivering nanomedicine to solid tumors. Nat Rev Clin Oncol. 2010; 7:653–664. [PubMed: 20838415]
12. Shields MA, Dangi-Garimella S, Redig AJ, Munshi HG. Biochemical role of the collagen-rich tumour microenvironment in pancreatic cancer progression. Biochem J. 2012; 441:541–552. [PubMed: 22187935]

13. Soto-Pantoja DR, Menon J, Gallagher PE, Tallant EA. Angiotensin-(1–7) inhibits tumor angiogenesis in human lung cancer xenografts with a reduction in vascular endothelial growth factor. Mol Cancer Ther. 2009; 8:1676–1683. [PubMed: 19509262]
14. Sethi T, Rintoul RC, Moore SM, MacKinnon AC, Salter D, Choo C, Chilvers ER, Dransfield I, Donnelly SC, Strieter R, Haslett C. Extracellular matrix proteins protect small cell lung cancer cells against apoptosis: a mechanism for small cell lung cancer growth and drug resistance in vivo. Nat Med. 1999; 5:662–668. [PubMed: 10371505]
15. Cook KL, Metheny-Barlow LJ, Tallant EA, Gallagher PE. Angiotensin-(1–7) reduces fibrosis in orthotopic breast tumors. Cancer Res. 2010; 70:8319–8328. [PubMed: 20837666]
16. Prud'homme GJ. Pathobiology of transforming growth factor beta in cancer, fibrosis and immunologic disease, and therapeutic considerations. Lab Invest. 2007; 87:1077–1091. [PubMed: 17724448]
17. Kaminska B, Wesolowska A, Danilkiewicz M. TGF beta signalling and its role in tumour pathogenesis. Acta Biochim Pol. 2005; 52:329–337. [PubMed: 15990918]
18. Reka AK, Kurapati H, Narala VR, Bommer G, Chen J, Standiford TJ, Keshamouni VG. Peroxisome proliferator-activated receptor-gamma activation inhibits tumor metastasis by antagonizing Smad3-mediated epithelial-mesenchymal transition. Mol Cancer Ther. 2010; 9:3221–3232. [PubMed: 21159608]
19. Ray DM, Myers PH, Painter JT, Hoenerhoff MJ, Olden K, Roberts JD. Inhibition of transforming growth factor-beta-activated kinase-1 blocks cancer cell adhesion, invasion, and metastasis. Br J Cancer. 2012; 107:129–136. [PubMed: 22644295]
20. Imamura T, Hikita A, Inoue Y. The roles of TGF-beta signaling in carcinogenesis and breast cancer metastasis. Breast Cancer. 2012; 19:118–124. [PubMed: 22139728]
21. Kano MR, Bae Y, Iwata C, Morishita Y, Yashiro M, Oka M, Fujii T, Komuro A, Kiyono K, Kaminishi M, Hirakawa K, Ouchi Y, Nishiyama N, Kataoka K, Miyazono K. Improvement of cancer-targeting therapy, using nanocarriers for intractable solid tumors by inhibition of TGF-beta signaling. Proc Natl Acad Sci U S A. 2007; 104:3460–3465. [PubMed: 17307870]
22. Lee CH, Kim HD, Shin SM, Kim SG. A Novel Mechanism of PPARgamma Regulation of TGFbeta1: Implication in Cancer Biology. PPAR Res. 2008; 2008:762398. [PubMed: 18615188]
23. Maejima Y, Okada H, Haraguchi G, Onai Y, Kosuge H, Suzuki J, Isobe M. Telmisartan, a unique ARB, improves left ventricular remodeling of infarcted heart by activating PPAR gamma. Lab Invest. 2011; 91:932–944. [PubMed: 21403641]
24. Benson SC, Pershadsingh HA, Ho CI, Chittiboyina A, Desai P, Pravenec M, Qi N, Wang J, Avery MA, Kurtz TW. Identification of telmisartan as a unique angiotensin II receptor antagonist with selective PPARgamma-modulating activity. Hypertension. 2004; 43:993–1002. [PubMed: 15007034]
25. Funao K, Matsuyama M, Kawahito Y, Sano H, Chargui J, Touraine JL, Nakatani T, Yoshimura R. Telmisartan as a peroxisome proliferator-activated receptor-gamma ligand is a new target in the treatment of human renal cell carcinoma. Mol Med Report. 2009; 2:193–198.
26. Lakshmanan AP, Watanabe K, Thandavarayan RA, Sari FR, Harima M, Giridharan VV, Soetikno V, Kodama M, Aizawa Y. Telmisartan attenuates oxidative stress and renal fibrosis in streptozotocin induced diabetic mice with the alteration of angiotensin-(1–7) mas receptor expression associated with its PPAR-gamma agonist action. Free Radic Res. 2011; 45:575–584. [PubMed: 21381899]
27. Geirsson A, Singh M, Ali R, Abbas H, Li W, Sanchez JA, Hashim S, Tellides G. Modulation of transforming growth factor-beta signaling and extracellular matrix production in myxomatous mitral valves by angiotensin II receptor blockers. Circulation. 2012; 126:S189–S197. [PubMed: 22965982]
28. Chen Y, Luo Q, Xiong Z, Liang W, Chen L. Telmisartan counteracts TGF-beta1 induced epithelial-to-mesenchymal transition via PPAR-gamma in human proximal tubule epithelial cells. Int J Clin Exp Pathol. 2012; 5:522–529. [PubMed: 22949934]
29. Gao D, Ning N, Hao G, Niu X. Pioglitazone attenuates vascular fibrosis in spontaneously hypertensive rats. PPAR Res. 2012; 2012:856426. [PubMed: 22550475]

30. Kociecka B, Surazynski A, Miltyk W, Palka J. The effect of Telmisartan on collagen biosynthesis depends on the status of estrogen activation in breast cancer cells. Eur J Pharmacol. 2010; 628:51–56. [PubMed: 19945454]

31. Rodrigues-Ferreira S, Abdelkarim M, Dillenburg-Pilla P, Luissint AC, di-Tommaso A, Deshayes F, Pontes CL, Molina A, Cagnard N, Letourneur F, Morel M, Reis RI, Casarini DE, Terris B, Couraud PO, Costa-Neto CM, Di Benedetto M, Nahmias C. Angiotensin II facilitates breast cancer cell migration and metastasis. PLoS One. 2012; 7:e35667. [PubMed: 22536420]

32. Gallagher PE, Cook K, Soto-Pantoja D, Menon J, Tallant EA. Angiotensin peptides and lung cancer. Curr Cancer Drug Targets. 2011; 11:394–404. [PubMed: 21395552]

33. Krishnan B, Torti FM, Gallagher PE, Tallant EA. Angiotensin-(1–7) reduces proliferation and angiogenesis of human prostate cancer xenografts with a decrease in angiogenic factors and an increase in sFlt-1. Prostate. 2013; 73:60–70. [PubMed: 22644934]

34. Menon J, Soto-Pantoja DR, Callahan MF, Cline JM, Ferrario CM, Tallant EA, Gallagher PE. Angiotensin-(1–7) inhibits growth of human lung adenocarcinoma xenografts in nude mice through a reduction in cyclooxygenase-2. Cancer Res. 2007; 67:2809–2815. [PubMed: 17363603]

35. George AJ, Thomas WG, Hannan RD. The renin-angiotensin system and cancer: old dog, new tricks. Nat Rev Cancer. 2010; 10:745–759. [PubMed: 20966920]

36. Rhodes DR, Ateeq B, Cao Q, Tomlins SA, Mehra R, Laxman B, Kalyana- Sundaram S, Lonigro RJ, Helgeson BE, Bhojani MS, Rehemtulla A, Kleer CG, Hayes DF, Lucas PC, Varambally S, Chinnaiyan AM. AGTR1 overexpression defines a subset of breast cancer and confers sensitivity to losartan, an AGTR1 antagonist. Proc Natl Acad Sci U S A. 2009; 106:10284–10289. [PubMed: 19487683]

37. Kosaka T, Miyajima A, Takayama E, Kikuchi E, Nakashima J, Ohigashi T, Asano T, Sakamoto M, Okita H, Murai M, Hayakawa M. Angiotensin II type 1 receptor antagonist as an angiogenic inhibitor in prostate cancer. Prostate. 2007; 67:41–49. [PubMed: 17044086]

38. Donovan D, Harmey JH, Toomey D, Osborne DH, Redmond HP, Bouchier-Hayes DJ. TGF beta-1 regulation of VEGF production by breast cancer cells. Ann Surg Oncol. 1997; 4:621–627. [PubMed: 9416408]

39. Krishnan B, Smith TL, Dubey P, Zapadka ME, Torti FM, Willingham MC, Tallant EA, Gallagher PE. Angiotensin-(1–7) attenuates metastatic prostate cancer and reduces osteoclastogenesis. Prostate. 2013; 73:71–82. [PubMed: 22644942]

40. Doi C, Egashira N, Kawabata A, Maurya DK, Ohta N, Uppalapati D, Ayuzawa R, Pickel L, Isayama Y, Troyer D, Takekoshi S, Tamura M. Angiotensin II type 2 receptor signaling significantly attenuates growth of murine pancreatic carcinoma grafts in syngeneic mice. BMC Cancer. 2010; 10:67. [PubMed: 20181281]

41. Pickel L, Matsuzuka T, Doi C, Ayuzawa R, Maurya DK, Xie SX, Berkland C, Tamura M. Overexpression of angiotensin II type 2 receptor gene induces cell death in lung adenocarcinoma cells. Cancer Biol Ther. 2010; 9

42. Arnold SA, Rivera LB, Carbon JG, Toombs JE, Chang CL, Bradshaw AD, Brekken RA. Losartan slows pancreatic tumor progression and extends survival of SPARC-null mice by abrogating aberrant TGFbeta activation. PLoS One. 2012; 7:e31384. [PubMed: 22348081]

43. Ichite N, Chougule M, Patel AR, Jackson T, Safe S, Singh M. Inhalation delivery of a novel diindolylmethane derivative for the treatment of lung cancer. Mol Cancer Ther. 2010; 9:3003–3014. [PubMed: 20978159]

44. Navab R, Strumpf D, Bandarchi B, Zhu CQ, Pintilie M, Ramnarine VR, Ibrahimov E, Radulovich N, Leung L, Barczyk M, Panchal D, To C, Yun JJ, Der S, Shepherd FA, Jurisica I, Tsao MS. Prognostic gene-expression signature of carcinoma-associated fibroblasts in non-small cell lung cancer. Proc Natl Acad Sci U S A. 2011; 108:7160–7165. [PubMed: 21474781]

45. Haubeiss S, Schmid JO, Murdter TE, Sonnenberg M, Friedel G, van der Kuip H, Aulitzky WE. Dasatinib reverses cancer-associated fibroblasts (CAFs) from primary lung carcinomas to a phenotype comparable to that of normal fibroblasts. Mol Cancer. 2010; 9:168. [PubMed: 20579391]

46. Chauhan VP, Popovic Z, Chen O, Cui J, Fukumura D, Bawendi MG, Jain RK. Fluorescent nanorods and nanospheres for real-time in vivo probing of nanoparticle shapedependent tumor penetration. Angew Chem Int Ed Engl. 2011; 50:11417–11420. [PubMed: 22113800]

47. McKee TD, Grandi P, Mok W, Alexandrakis G, Insin N, Zimmer JP, Bawendi MG, Boucher Y, Breakefield XO, Jain RK. Degradation of fibrillar collagen in a human melanoma xenograft improves the efficacy of an oncolytic herpes simplex virus vector. Cancer Res. 2006; 66:2509–2513. [PubMed: 16510565]

48. Minowa T, Kawano K, Kuribayashi H, Shiraishi K, Sugino T, Hattori Y, Yokoyama M, Maitani Y. Increase in tumour permeability following TGF-beta type I receptor-inhibitor treatment observed by dynamic contrast-enhanced MRI. Br J Cancer. 2009; 101:1884–1890. [PubMed: 19888220]

49. Ishiguro H, Ishiguro Y, Kubota Y, Uemura H. Regulation of prostate cancer cell growth and PSA expression by angiotensin II receptor blocker with peroxisome proliferator-activated receptor gamma ligand like action. Prostate. 2007; 67:924–932. [PubMed: 17440964]

50. Reka AK, Goswami MT, Krishnapuram R, Standiford TJ, Keshamouni VG. Molecular cross-regulation between PPAR-gamma and other signaling pathways: implications for lung cancer therapy. Lung Cancer. 2011; 72:154–159. [PubMed: 21354647]

51. Sipahi I, Debanne SM, Rowland DY, Simon DI, Fang JC. Angiotensin-receptor blockade and risk of cancer: meta-analysis of randomised controlled trials. Lancet Oncol. 2010; 11:627–636. [PubMed: 20542468]

52. Znati CA, Rosenstein M, McKee TD, Brown E, Turner D, Bloomer WD, Watkins S, Jain RK, Boucher Y. Irradiation reduces interstitial fluid transport and increases the collagen content in tumors. Clin Cancer Res. 2003; 9:5508–5513. [PubMed: 14654530]

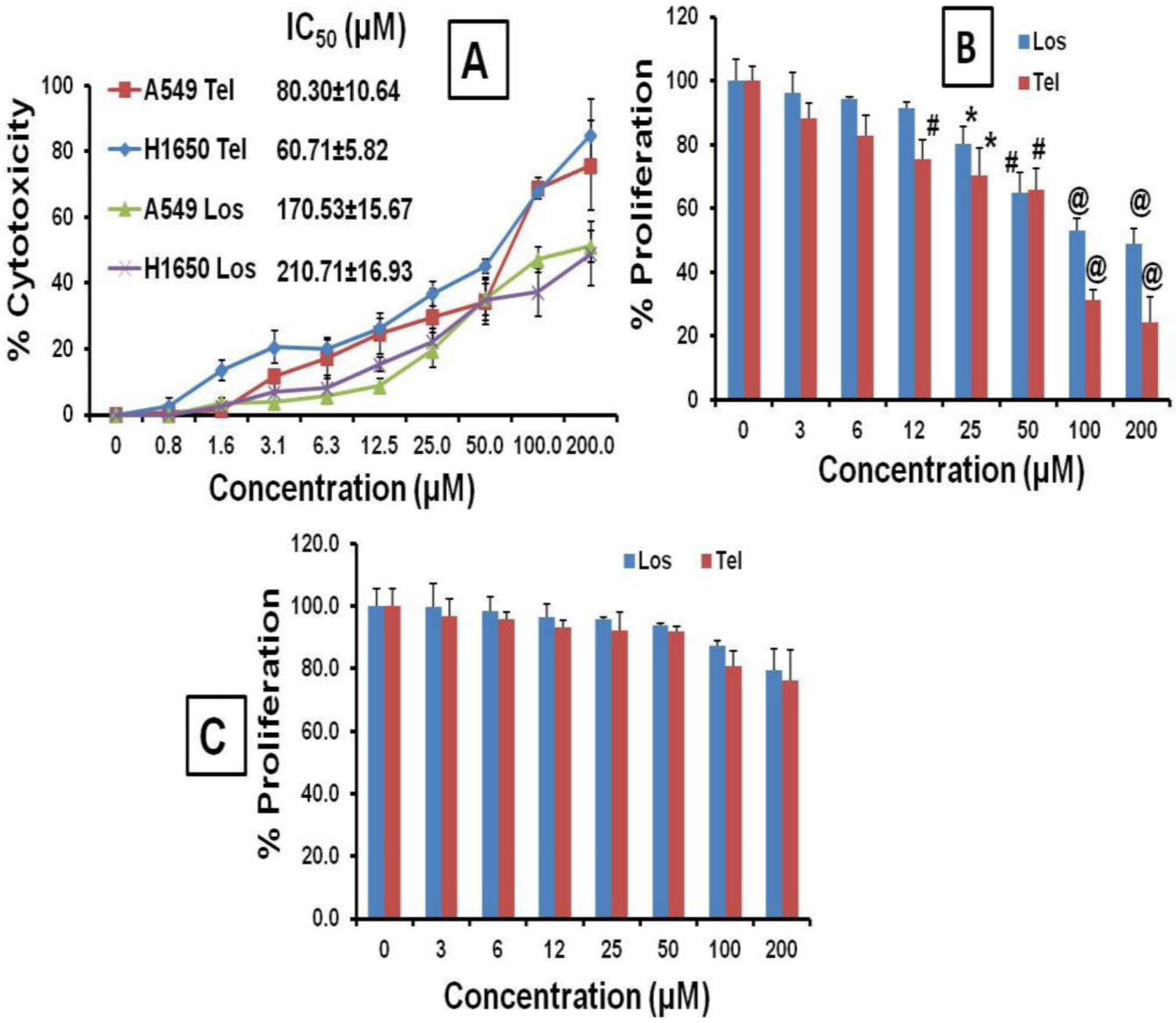

Figure 1.

In vitro anticancer effects: **(A)** Cytotoxicity of Losartan and Telmisartan on A549 and H1650 NCCLCs 72 h after the treatment, IC_{50} values were calculated. **(B)** Effect of Los and Tel on proliferation of A549 cells. **(C)** Effect of Los and Tel on proliferation of normal lung fibroblasts WI-38. Each data point is represent as mean ± sem (n=6–8). *P<0.05, #P<0.01 and @P<0.001 Vs respective controls.

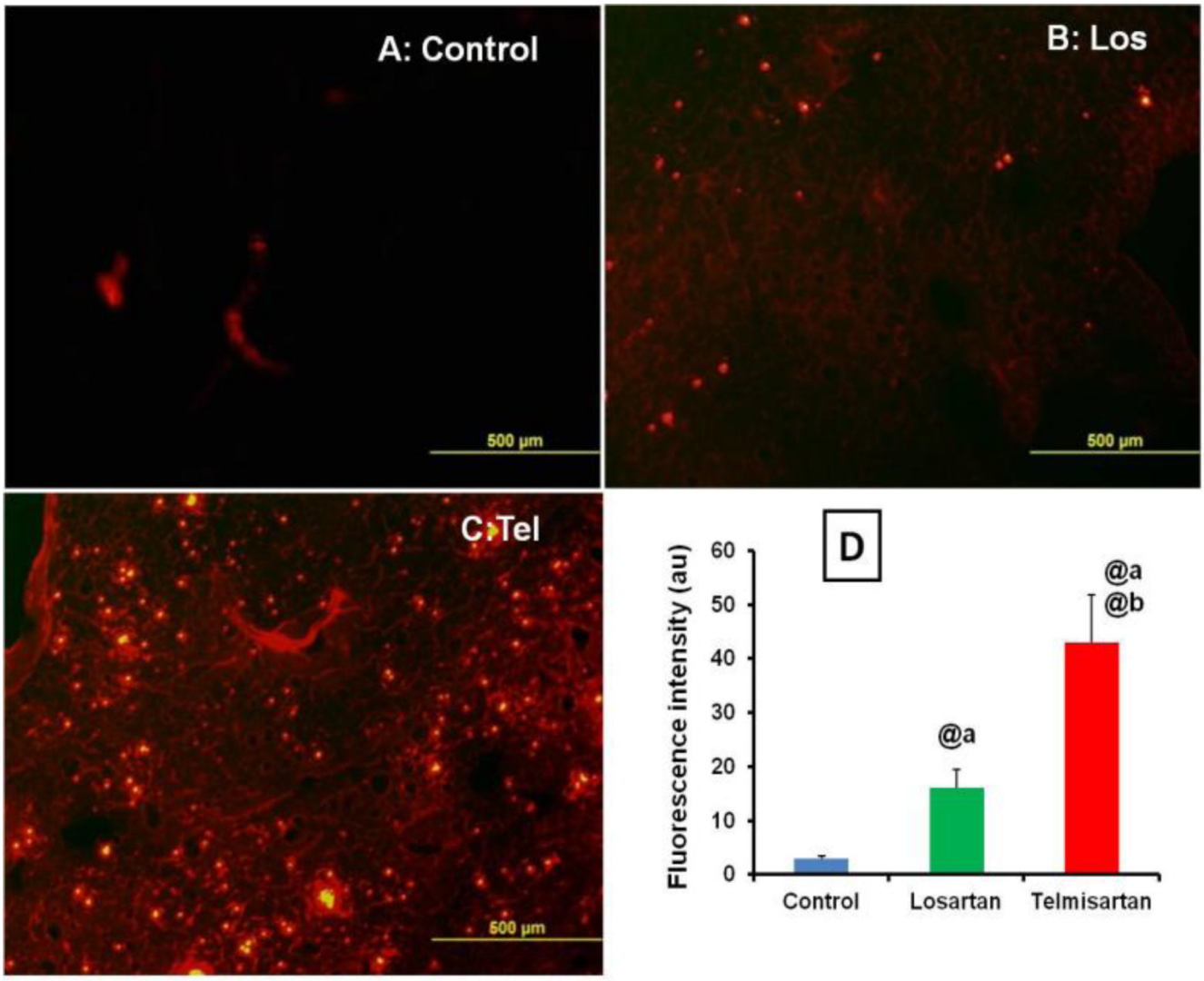

Figure 2.

Nanoparticles intratumoral distribution: Effect of inhalation treatment of Los and Tel on intratumoral distribution of FPNPs in **(A)** Control tumor **(B)** Losartan **(C)** Telmisartan and **(D)** Quantitative analysis of nanoparticles distribution in arbitrary units. Values were expressed as mean ± sem (n=3). @ $P<0.001$ **a** Vs control and **b** Vs Los group.

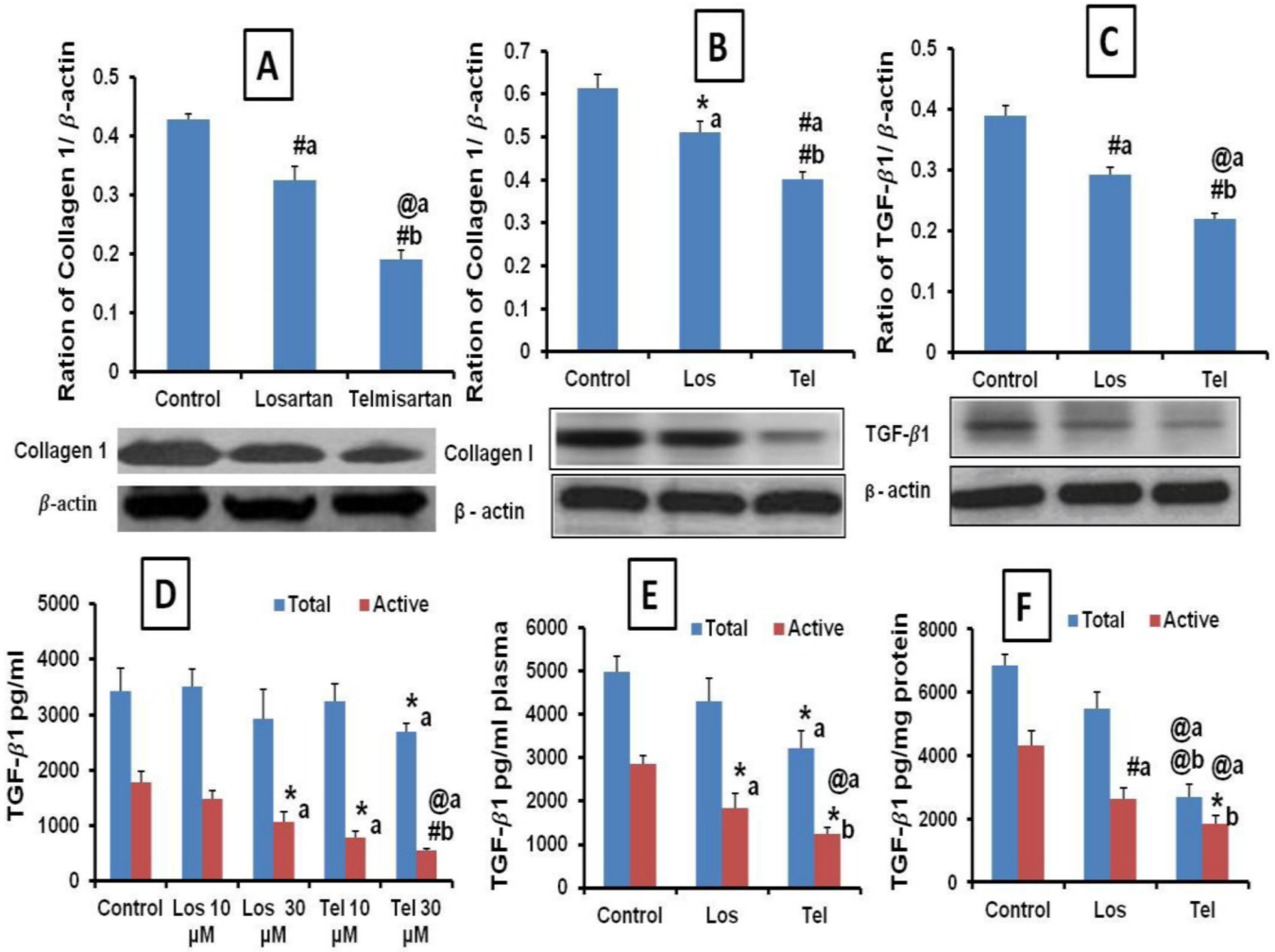

Figure 3.

Effect of inhalation delivery of Los and Tel on tumor collagen and TGF-β expression: Western blot images and densitometric analysis of tumor collagen 1 expression in **(A)** orthotopic tumors **(B)** metastatic tumors. **(C)** Western blot analysis of active TGF-β1 expression in orthotopic tumors. **(D)** Quantification of TGF-β1 total and active levels in invitro cell culture supernatants after treatment with Los and Tel 10 and 30 μM. **(E)** TGF-β1 total and active levels in plasma and **(F)** TGF β1 total and active levels in tumor lysates estimated by ELISA method. Each data point was represented as mean ± sem (n=3). *P<0.05, #P<0.01 and @P<0.001 **a** Vs control and **b** Vs Los group.

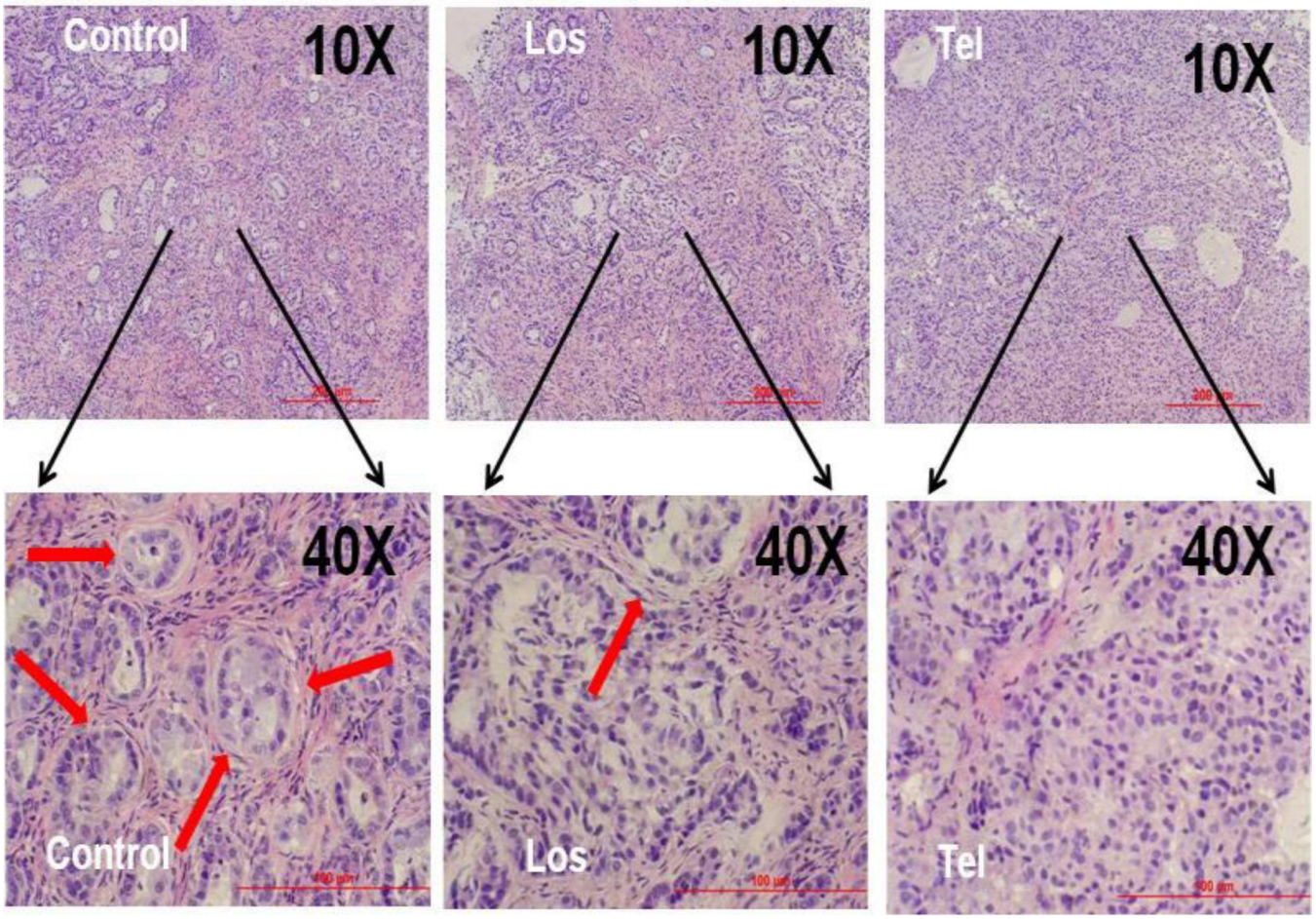

Figure 4.
Representative microscopic images of histopathological analysis of orthotopic tumors at 10X and 40X magnification. Red solid arrows indicate the collagen induced compartmentalization of Lung tumors, which are significantly decreased in Los and disappeared in Tel treated groups.

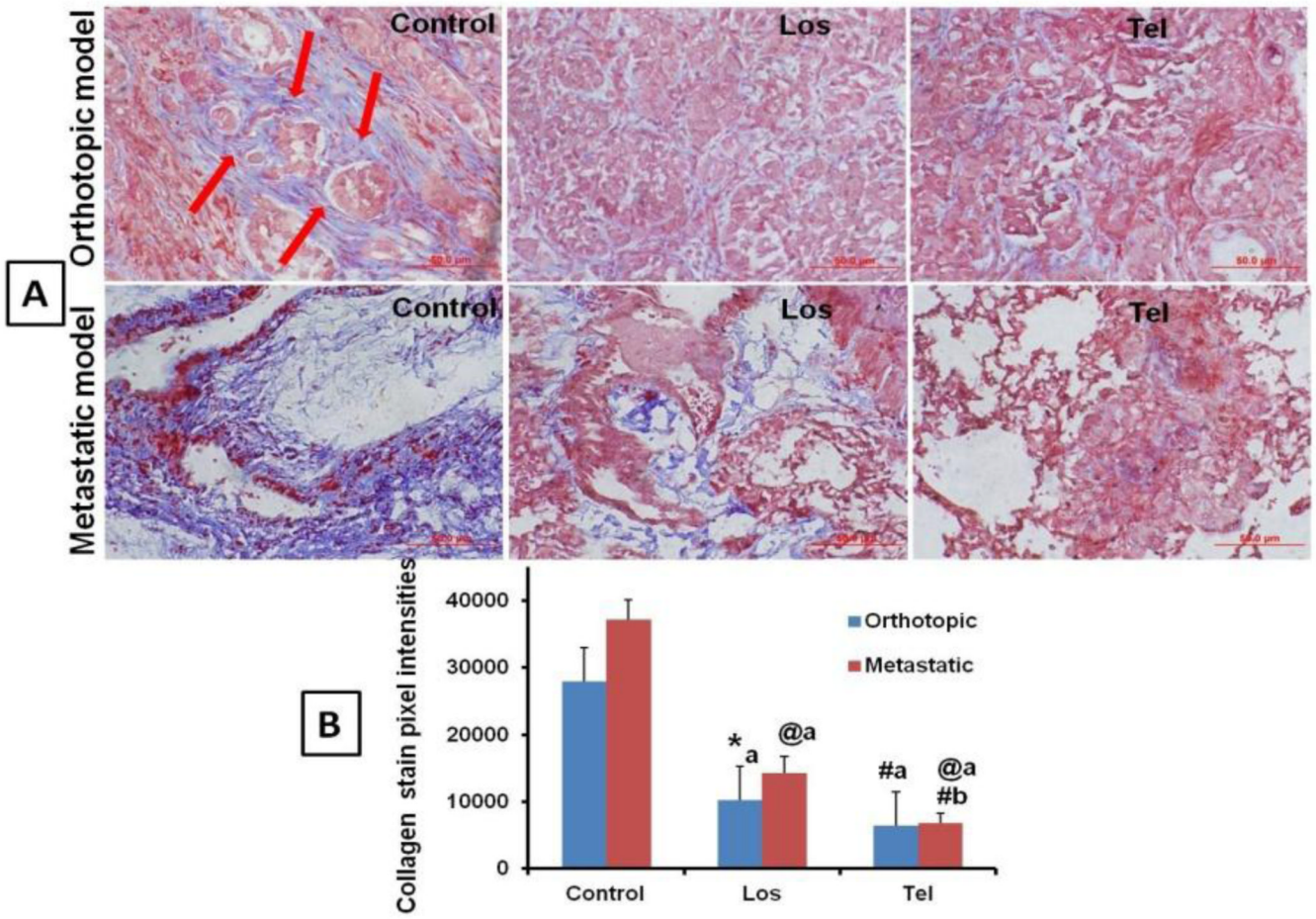

Figure 5.

Masson trichrome staining: **(A)** Effect of Los and Tel on collagen expression in orthotopic and metastatic lung tumor sections, blue color staining indicates the collagen expression. As observed in histopathology, blue color staining forming compartments suggest that collagen is involved in the tumor compartmentalization (Solid arrows). **(B)** Quantification of Masson trichrome stained collagen expression, collagen expression was significantly decreased in Los and Tel treated groups. Each data point was represented as mean ± sem (n=3). *P<0.05, #P<0.01 and @P<0.001 **a** Vs control and **b** Vs Los group.

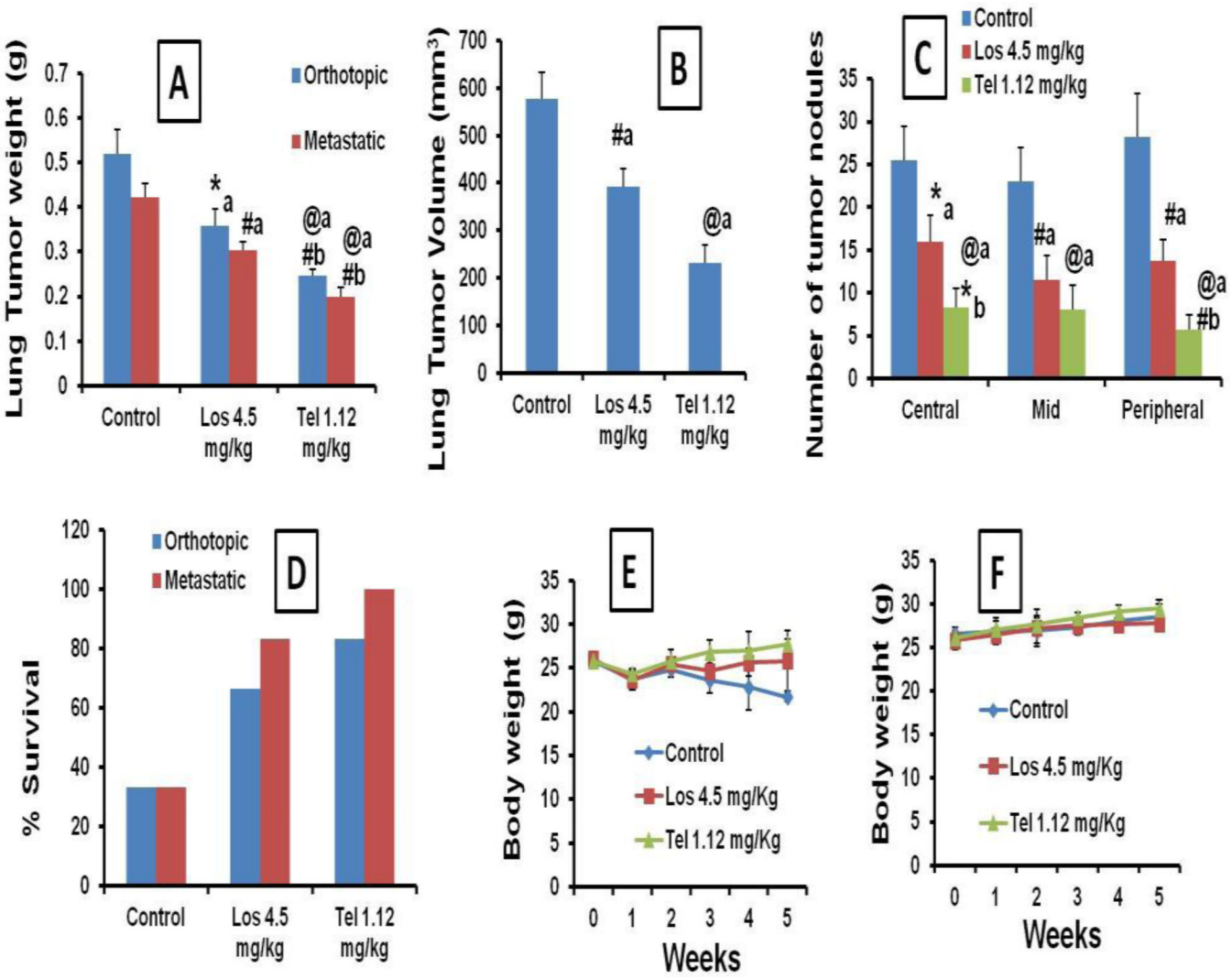

Figure 6.

Anticancer effects of Los and Tel upon inhalation delivery: **(A)** Lung tumor weights in orthotopic and metastatic models. **(B)** Effect of Los and Tel on tumor volumes in orthotopic tumors. **(C)** Effect of Los and Tel on lung tumor nodule number in metastatic lung tumor model. **(D)** Survival rates of orthotopic and metastatic tumor bearing animals during 5 weeks, upon inhalation treatment with Los and Tel. Body weight changes in inhalation Los and Tel treated orthotopic **(E)** and metastatic **(F)** tumor models. Each data point was represented as mean ± sem (n=3). *P<0.05, #P<0.01 and @P<0.001 **a** Vs control and **b** Vs Los groups.

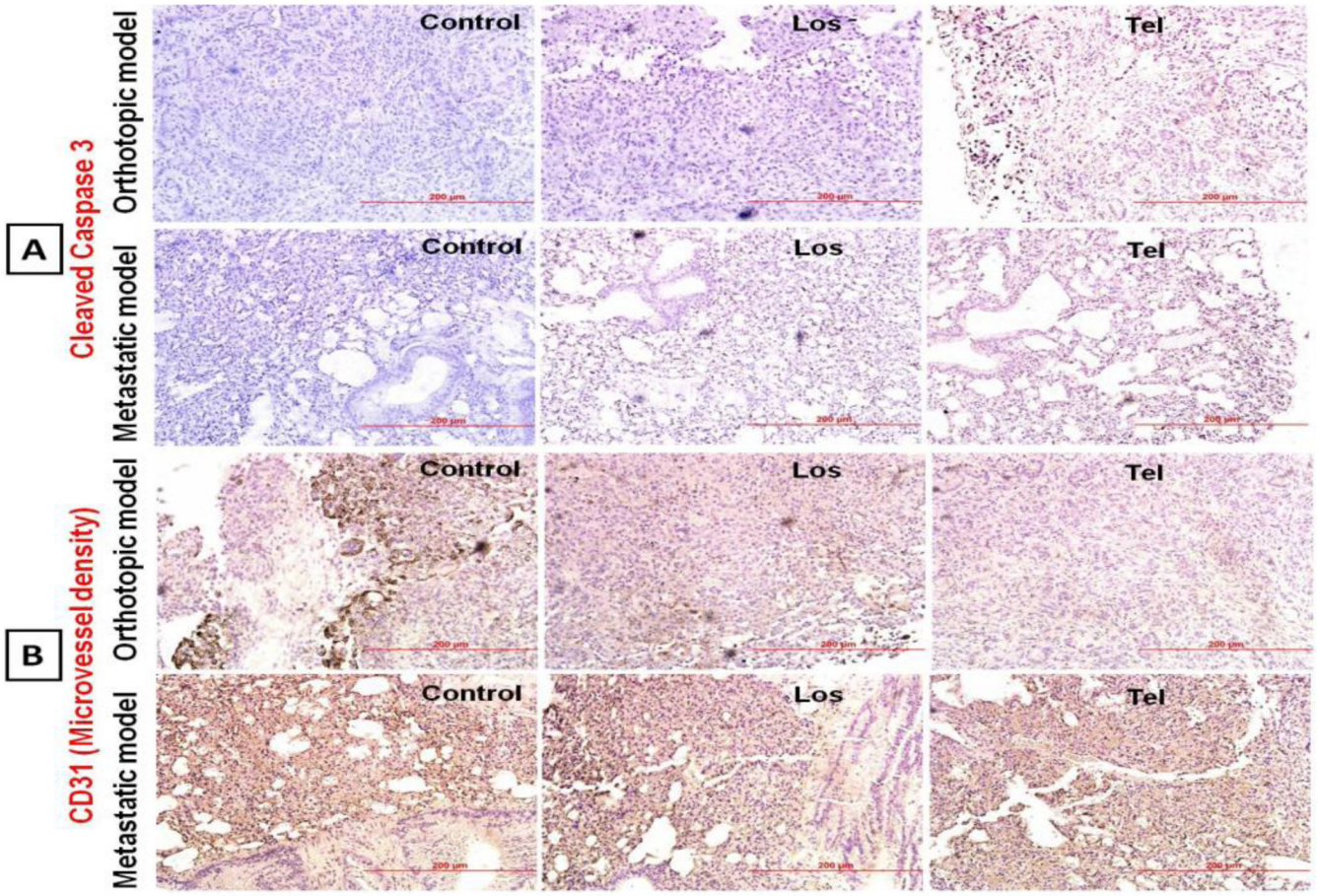

Figure 7.

Immunohistochemical analysis of tumor sections: Representative microscopic images of immunohistochemical analysis of Cleaved caspase 3 and CD31 based microvessel density (MCD) expression in orthotopic and metastatic tumor models treated with Los and Tel by inhalation route. **(A)** In cleaved caspase 3, decreased brown colored apoptotic cells were noticed in Los and Tel treated groups, suggesting the role of apoptosis in anticancer effects. **(B)** In CD31 based MVD analysis suggests that large numbers of microvessel are observed in untreated control tumors.

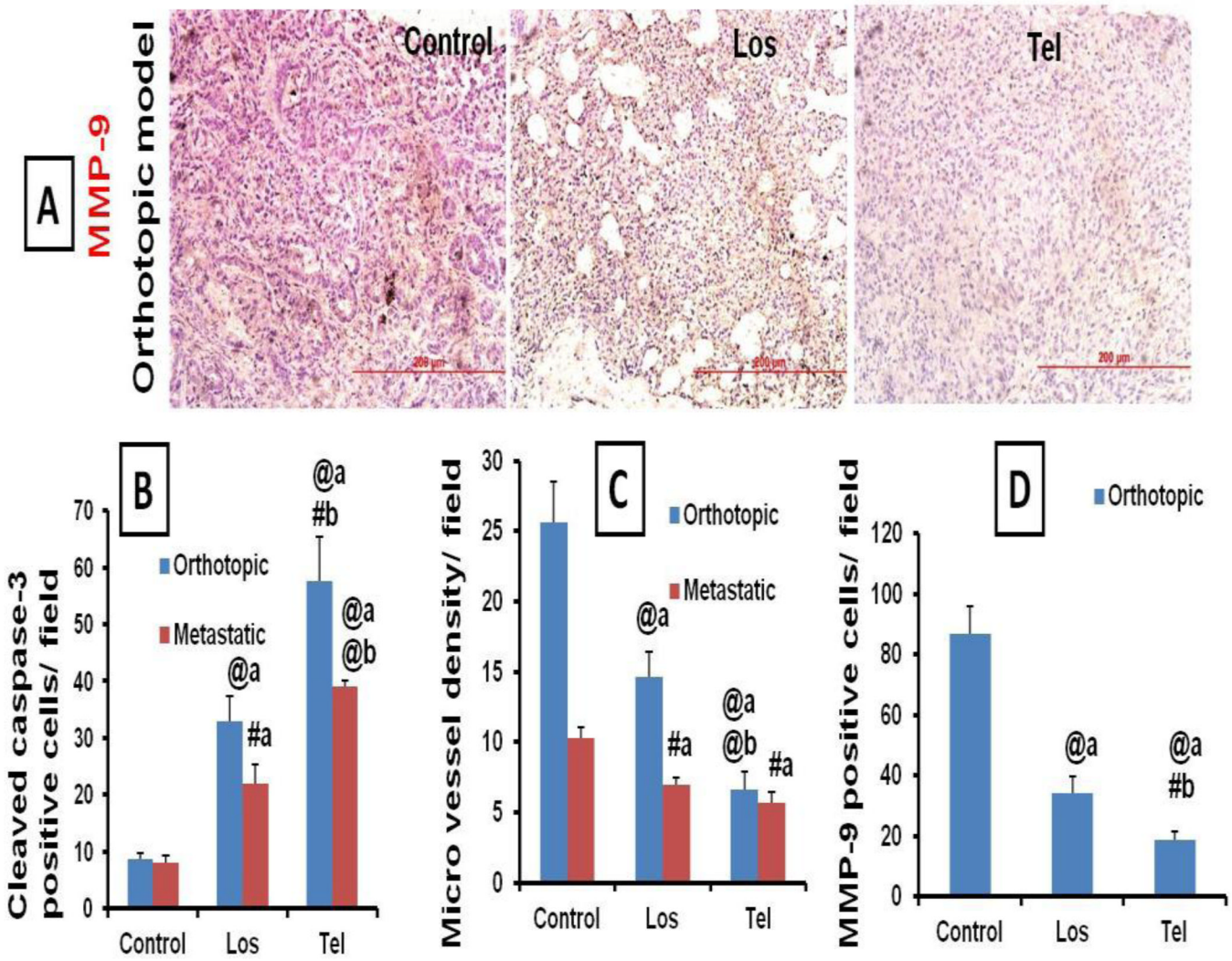

Figure 8.

Immunohistochemical analysis of tumor sections: **(A)** Representative microscopic images of Immunohistochemical analysis of MMP-9 in orthotopic tumor model treated with Los and Tel. Vast number of MMP-9 positive cells (Brown colored) was observed in untreated control tumors. Quantitative IHC analysis of **(B)** Cleaved caspase 3, **(C)** MVD and **(D)** MMP-9 expressions in various groups after treatment with Los and Tel. The averages of 10 fields per slide, 3 slides from each group were studied for the IHC analysis. Each data point was represented as mean ± sem (n=3). #P<0.01 and @P<0.001 **a** Vs control and **b** Vs Los group.

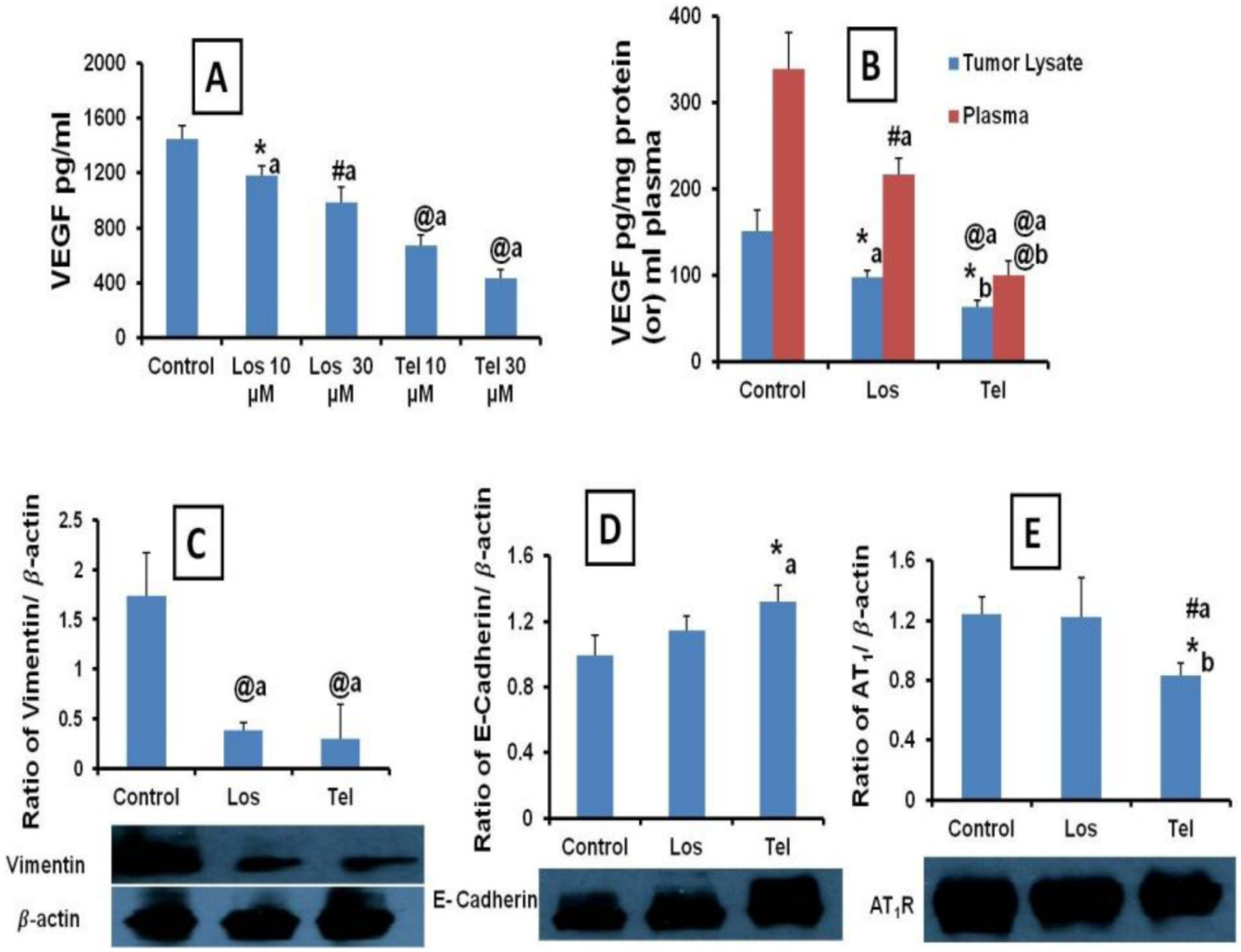

Figure 9.

Quantification of VEGF levels by ELISA method: **(A)** Effect of Los and Tel on VEGF expression in invitro A549 cells. **(B)** VEGF levels in tumor lysates and plasma after inhalation treatment with Los and Tel. Western blot images and densitometric analysis in orthotopic lung tumors treated with Los and Tel, **(C)** Vimentin **(D)** E-Cadherin and **(E)** AT_1 receptors expressions. Each data point was represented as mean ± sem (n=3). *P<0.05, #P<0.01 and @P<0.001 **a** Vs control and **b** Vs Los group.

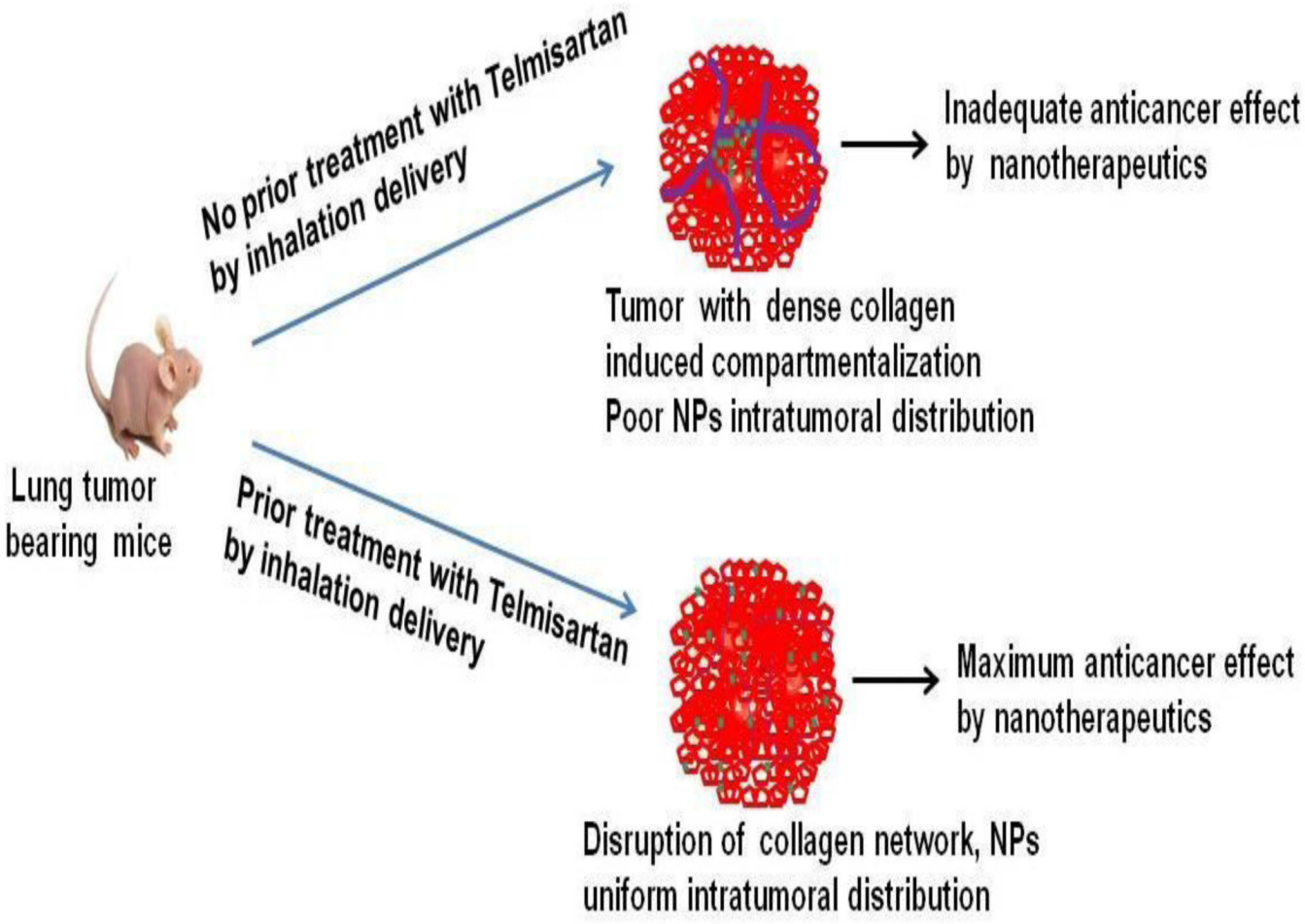

Figure 10.
Schematic representation of inhalation use of Tel to reduce tumor fibrosis and increase nanoparticle intratumoral distribution.